

## Supplementary Information For

### **Synergy of tellurium and defects in control of activity of phosphorene for oxygen evolution and reduction reactions**

Junfu Zhu,<sup>a</sup> Xingxing Jiang,<sup>a</sup> Ye Yang,<sup>a</sup> Qinjun Chen,<sup>a</sup> Xiong-Xiong Xue,<sup>\*a</sup> Keqiu Chen<sup>a</sup> and Yexin Feng<sup>\*ab</sup>

*<sup>a</sup>School of Physics and Electronics, Hunan University, Changsha 410082, People's Republic of China*

*<sup>b</sup>Hunan Provincial Key Laboratory of Low-Dimensional Structural Physics & Devices, Hunan University, Changsha 410082, People's Republic of China*

E-mail: xxxue@hnu.edu.cn, yexinfeng@pku.edu.cn

## Supplementary Text

In our work, the four-electron OER and ORR reactions are investigated. In alkaline environment, OER could occur in the following:<sup>1</sup>



where \* denotes absorption sites on the surface; (l) and (g) indicate the liquid and gas phases, respectively; OH\*, O\* and OOH\* are absorbed intermediates on the surface. The ORR reaction is the opposite process of OER from Eq. (S4) to (S1).

For the OER reaction, the overpotential  $\eta^{\text{OER}}$  can be evaluated from the Gibbs free energy differences of each step as following:<sup>1</sup>

$$G^{\text{OER}} = \max \{ \Delta G_1, \Delta G_2, \Delta G_3, \Delta G_4 \} \quad (\text{S5})$$

$$\eta^{\text{OER}} = G^{\text{OER}} / \text{e} - 0.402\text{V} \quad (\text{S6})$$

For the ORR reaction, the overpotential  $\eta^{\text{ORR}}$  can be evaluated as following:

$$G^{\text{ORR}} = \min \{ \Delta G_1, \Delta G_2, \Delta G_3, \Delta G_4 \} \quad (\text{S7})$$

$$\eta^{\text{ORR}} = 0.402\text{V} - G^{\text{ORR}} / \text{e} \quad (\text{S8})$$

where,  $\Delta G_1$ ,  $\Delta G_2$ ,  $\Delta G_3$ , and  $\Delta G_4$  are the Gibbs free energy of reactions (S1)-(S4) at  $U = 0$ , respectively. 0.402 V is the equilibrium potential at the standard condition and under the alkaline environment with pH = 14.

**Table. S1** Zero-point energy (ZPE) and entropic correction (TS) for H<sub>2</sub>O, H<sub>2</sub>, O\*, OH\*, OOH\* at T = 298.15 K. The values of H<sub>2</sub>O and H<sub>2</sub> molecules in gas phase are taken from the NIST database.<sup>2</sup> For the absorbed intermediates O\*, OH\* and OOH\*, the ZPE and TS are evaluated from the vibrational frequencies on selected Te sites of SW2-Te<sub>p</sub><sup>1</sup> and Pri-Te<sub>p</sub><sup>3</sup>, which give the similar results. The same values of absorbed species are used for all the structures, similar as previous work.<sup>3</sup>

Species	ZPE (eV)	TS (eV)
H <sub>2</sub> O	0.56	0.67
H <sub>2</sub>	0.27	0.41
O*	0.08	0.056
OH*	0.381	0.074
OOH*	0.461	0.142

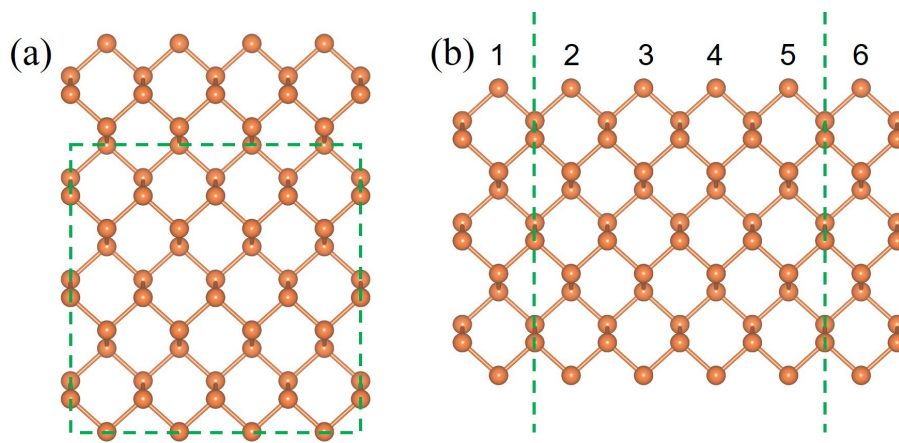


**Fig. S1** Atomic structures of (a)  $4 \times 4$  phosphorene supercell and (b) zigzag nanoribbon with the width of 6 zigzag chains. Green dotted lines denote the cropped part shown in manuscript and supplementary information.

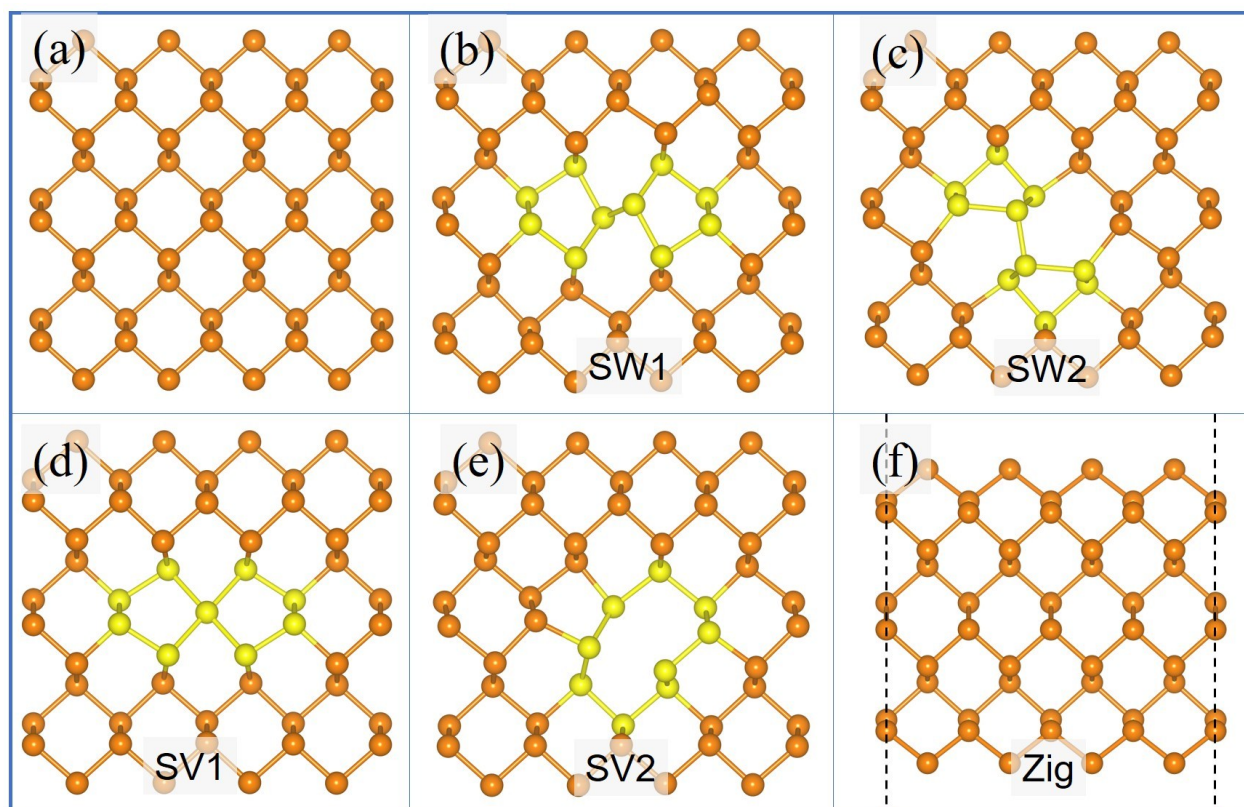


**Fig. S2** Atomic structures of (a) Pristine phosphene, Stone–Wales defects of (b) SW1 and (c) SW2, single vacancy defects of (d) SV1 and (e) SV2, and (f) Zigzag nanoribbon.

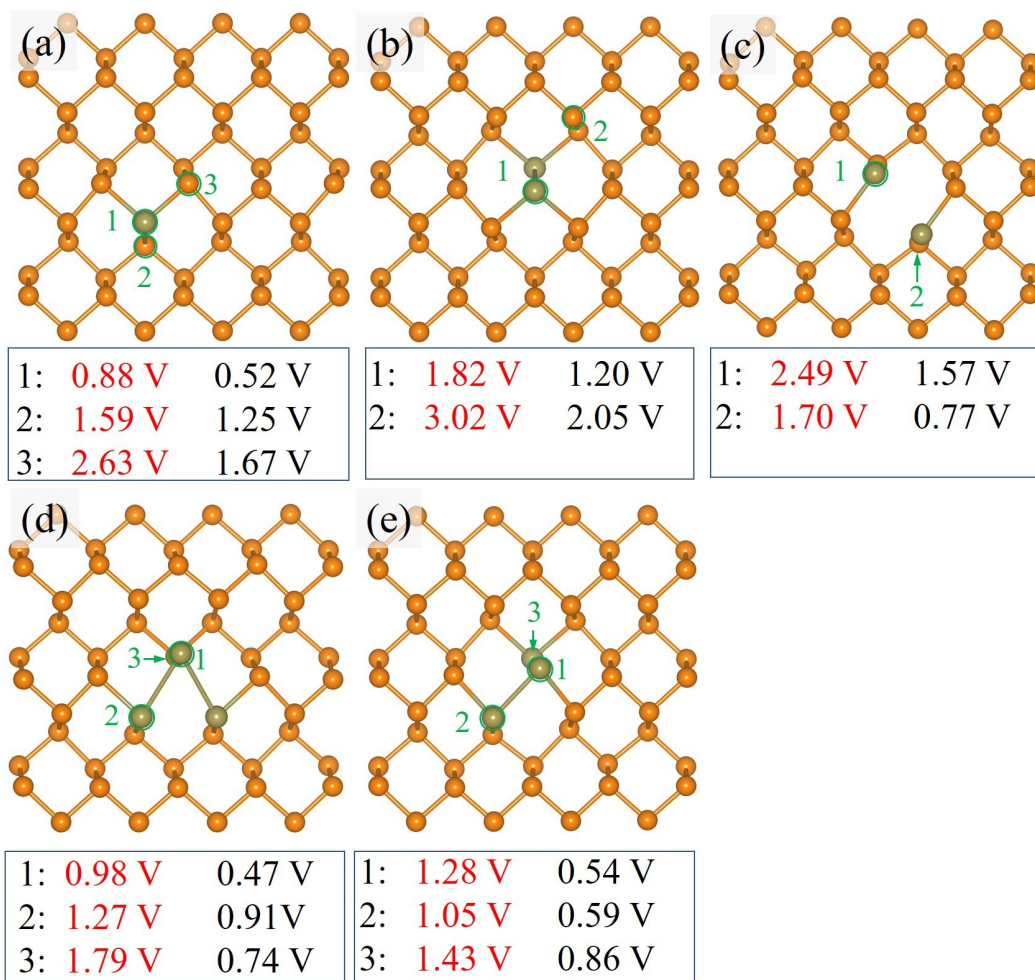


**Fig. S3** Atomic structures for pristine phosphene with doped Te atoms of Pri- (a)  $\text{Te}_p^1$ , (b)  $\text{Te}_p^2\text{-a}$ , (c)  $\text{Te}_p^2\text{-b}$ , (d)  $\text{Te}_p^3\text{-a}$  and (e)  $\text{Te}_p^3\text{-b}$ . For structures with 2 and 3 Te atoms, we only select two structures with lower energy to learn catalytic activity. The calculated OER (in red) and ORR (in black) overpotentials at representative active sites (green dashed circles and arrows) are listed below each diagram.

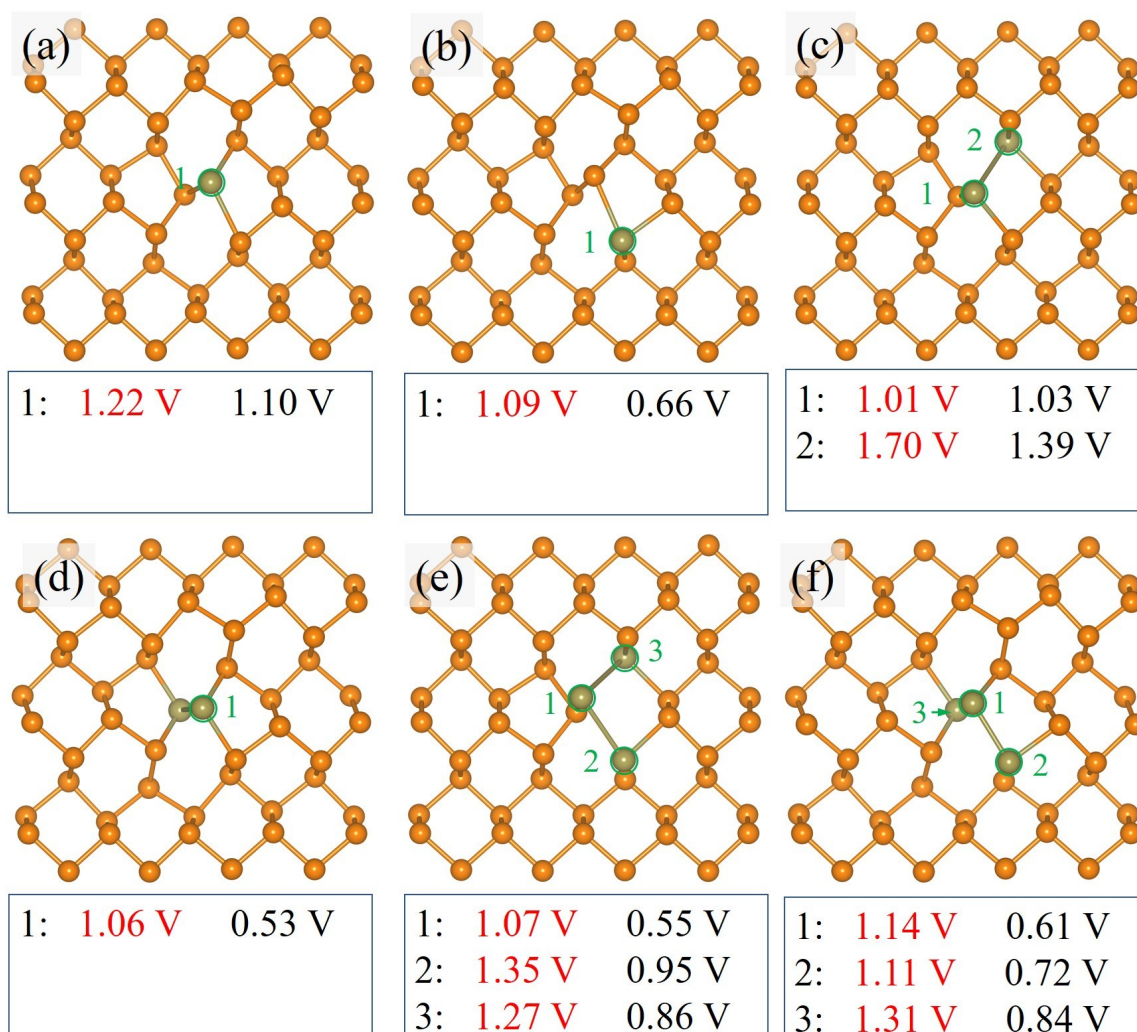


**Fig. S4** Atomic structures for Stone–Wales defects with doped Te atoms of SW1- (a)  $\text{Te}_p^1\text{-a}$ , (b)  $\text{Te}_p^1\text{-b}$ , (c)  $\text{Te}_p^2\text{-a}$ , (d)  $\text{Te}_p^2\text{-b}$ , (e)  $\text{Te}_p^3\text{-a}$  and (f)  $\text{Te}_p^3\text{-b}$ . We only select two structures with lower energy to learn catalytic activity. The calculated OER (in red) and ORR (in black) overpotentials at the representative active sites (green dashed circles and arrows) are listed below each diagram.

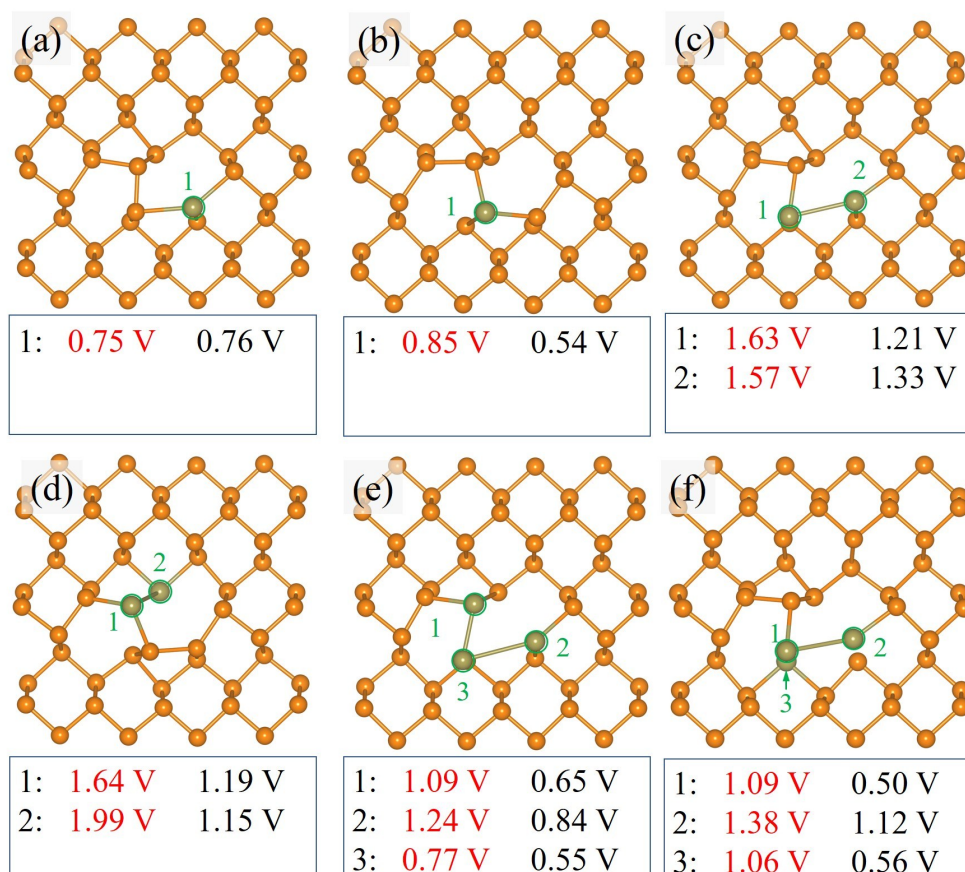


**Fig. S5** Atomic structures for Stone–Wales defects with doped Te atoms of SW2- (a)  $\text{Te}_p^1\text{-a}$ , (b)  $\text{Te}_p^1\text{-b}$ , (c)  $\text{Te}_p^2\text{-a}$ , (d)  $\text{Te}_p^2\text{-b}$ , (e)  $\text{Te}_p^3\text{-a}$  and (f)  $\text{Te}_p^3\text{-b}$ . We only select two structures with lower energy to learn catalytic activity. The calculated OER (in red) and ORR (in black) overpotentials at the representative active sites (green dashed circles and arrows) are listed below each diagram.

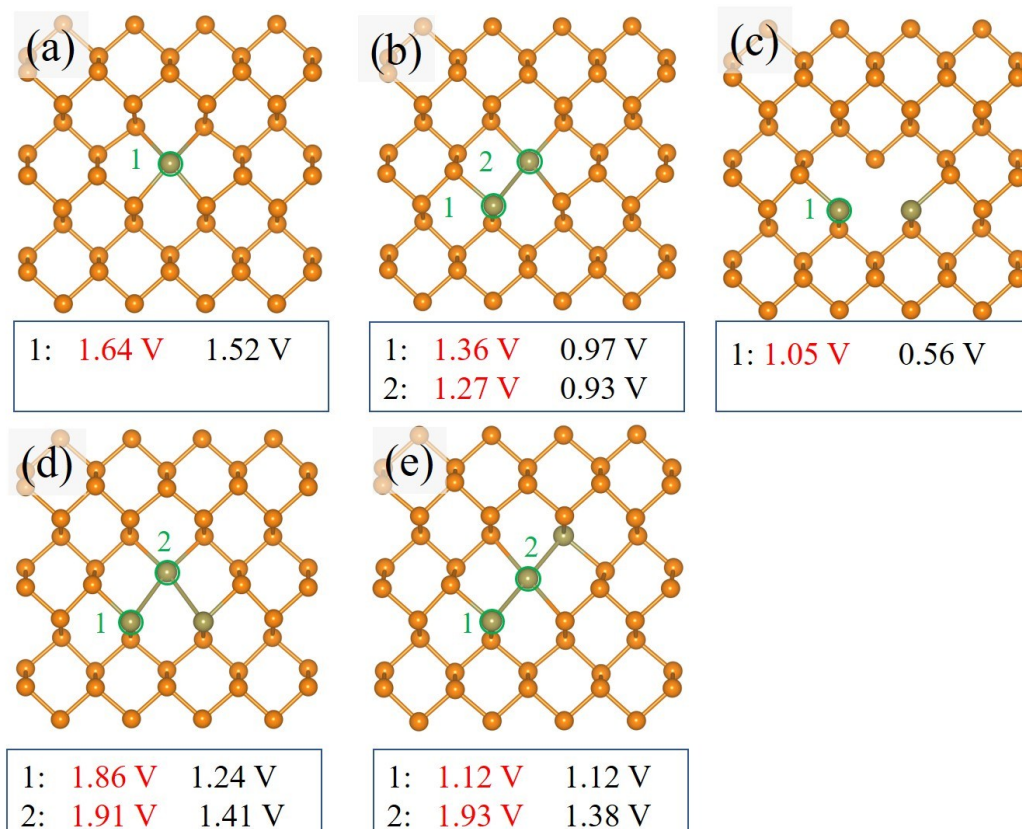


**Fig. S6** Atomic structures for single vacancy defects with doped Te atoms of SV1- (a)  $\text{Te}_p^1\text{-a}$ , (b)  $\text{Te}_p^1\text{-b}$ , (c)  $\text{Te}_p^2\text{-a}$ , (d)  $\text{Te}_p^2\text{-b}$ , (e)  $\text{Te}_p^3\text{-a}$  and (f)  $\text{Te}_p^3\text{-b}$ . We only select two structures with lower energy to learn catalytic activity. The calculated OER (in red) and ORR (in black) overpotentials at the representative active sites (green dashed circles and arrows) are listed below each diagram.

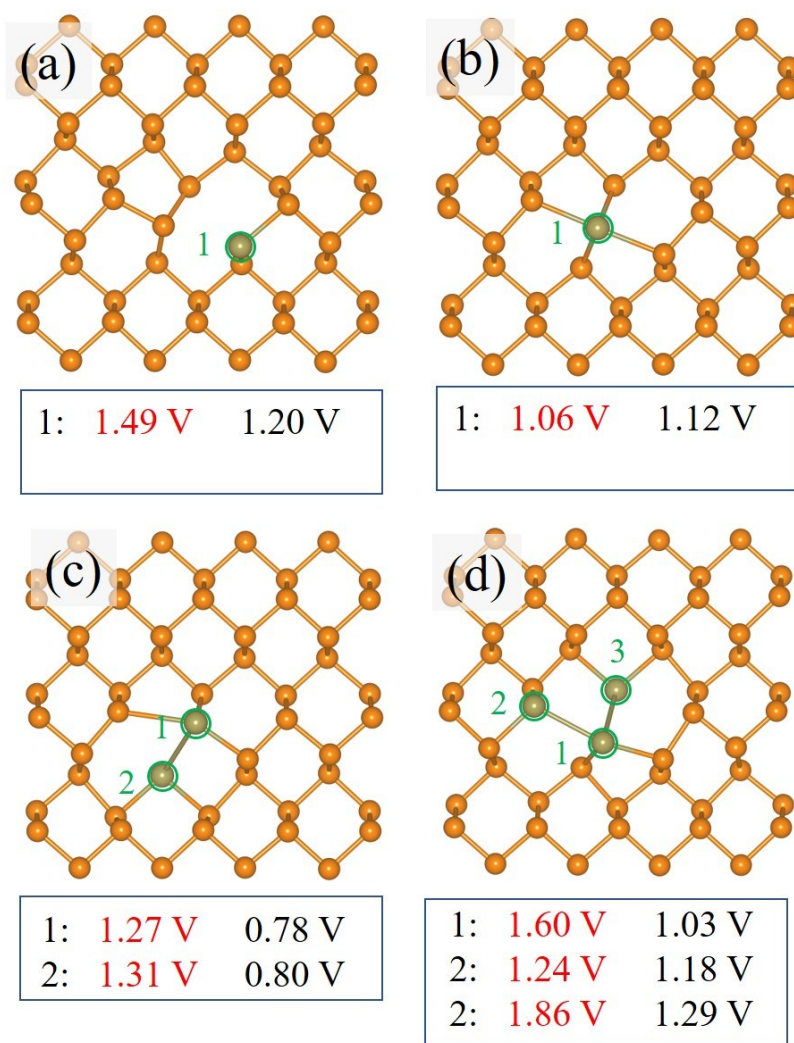


**Fig. S7** Atomic structures for single vacancy defects with doped Te atoms of SV2- (a)  $\text{Te}_p^1$ , (b)  $\text{Te}_p^2$ , (c)  $\text{Te}_p^3$ .

The calculated OER (in red) and ORR (in black) overpotentials at the representative active sites (green dashed circles and arrows) are listed below each diagram.

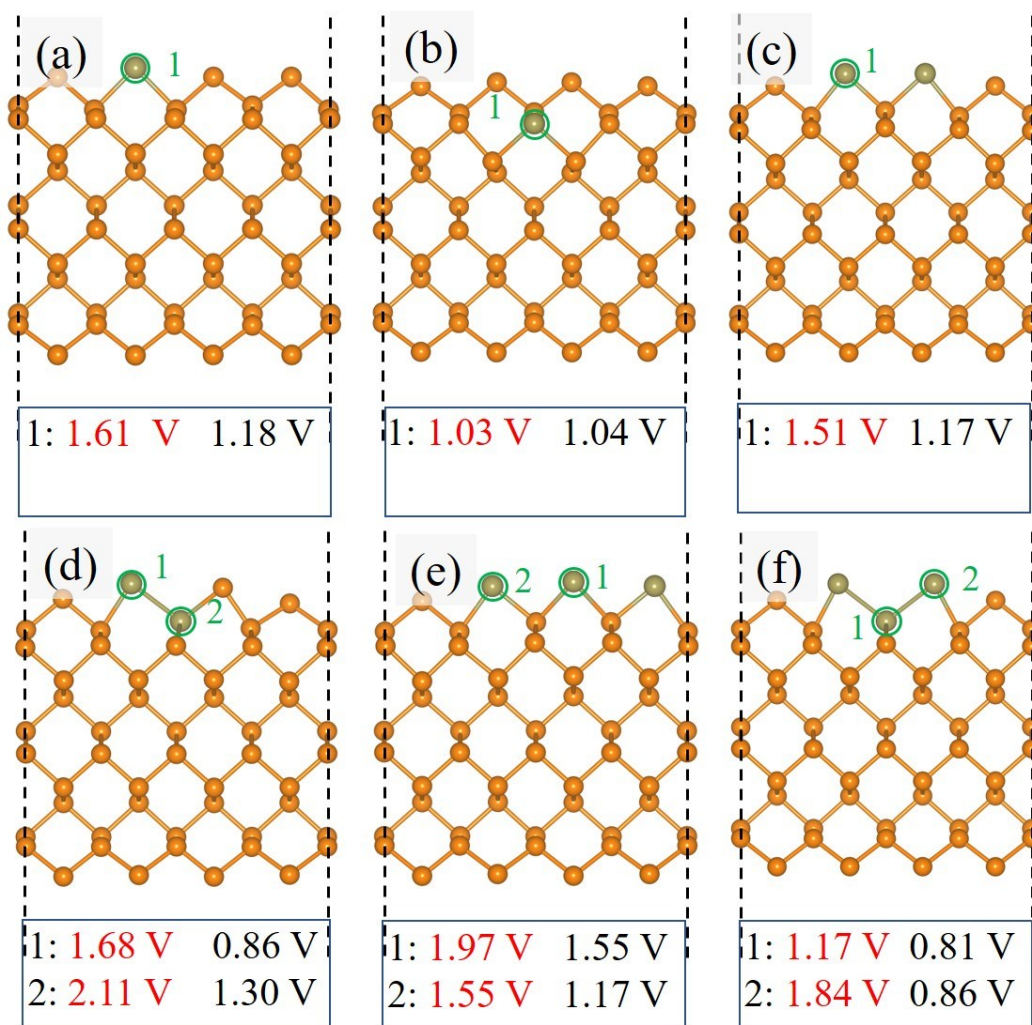


**Fig. S8** Atomic structures for zigzag nanoribbon with doped Te atoms of Zig- (a)  $\text{Te}_p^1\text{-a}$ , (b)  $\text{Te}_p^1\text{-b}$ , (c)  $\text{Te}_p^2\text{-a}$ , (d)  $\text{Te}_p^2\text{-b}$ , (e)  $\text{Te}_p^3\text{-a}$  and (f)  $\text{Te}_p^3\text{-b}$ . We only select two structures with lower energy to learn catalytic activity. The calculated OER (in red) and ORR (in black) overpotentials at the representative active sites (green dashed circles and arrows) are listed below each diagram.

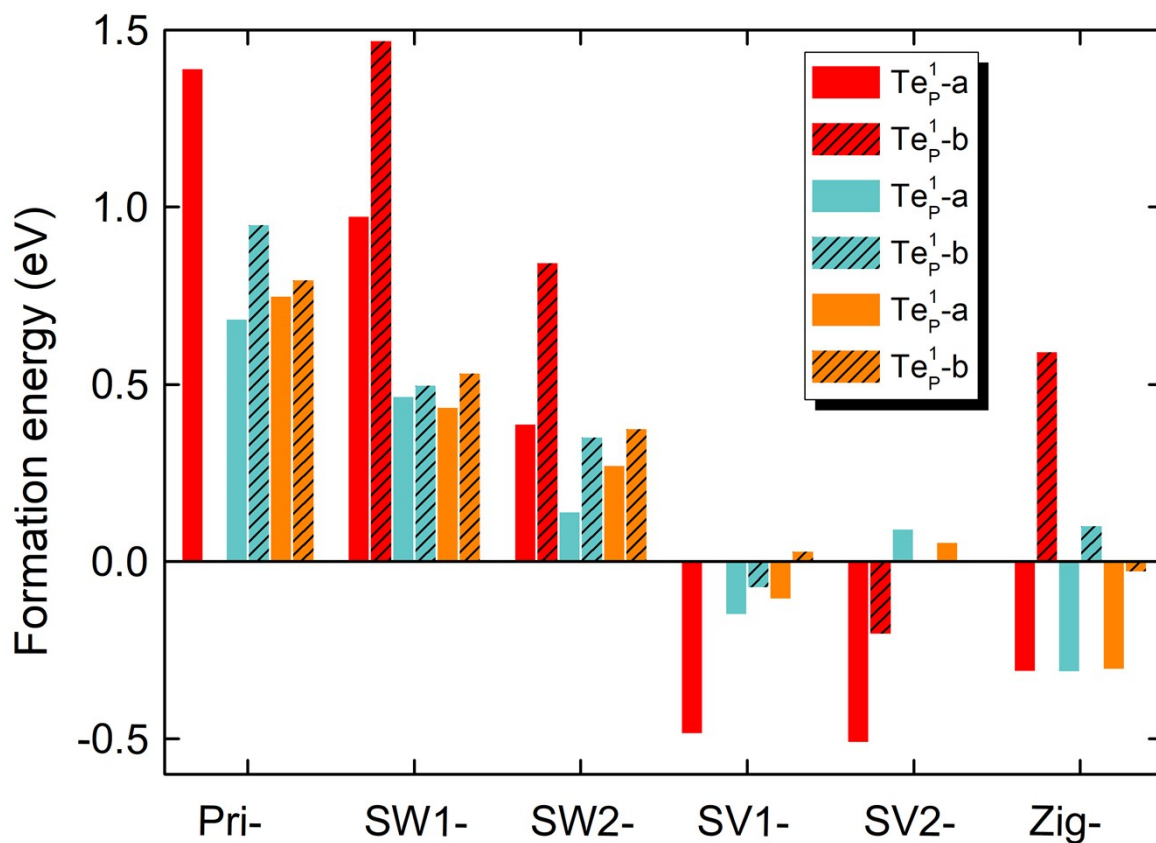


**Fig. S9** The formation energies ( $E_f$ 's) per Te atom of  $Te_p^x$  ( $x=1\sim 3$ ) clusters in pristine phosphene (Pri-), defective phosphene (SW- and SV-), and zigzag nanoribbon (Zig-). Two kinds of structures with the lower energy are shown.

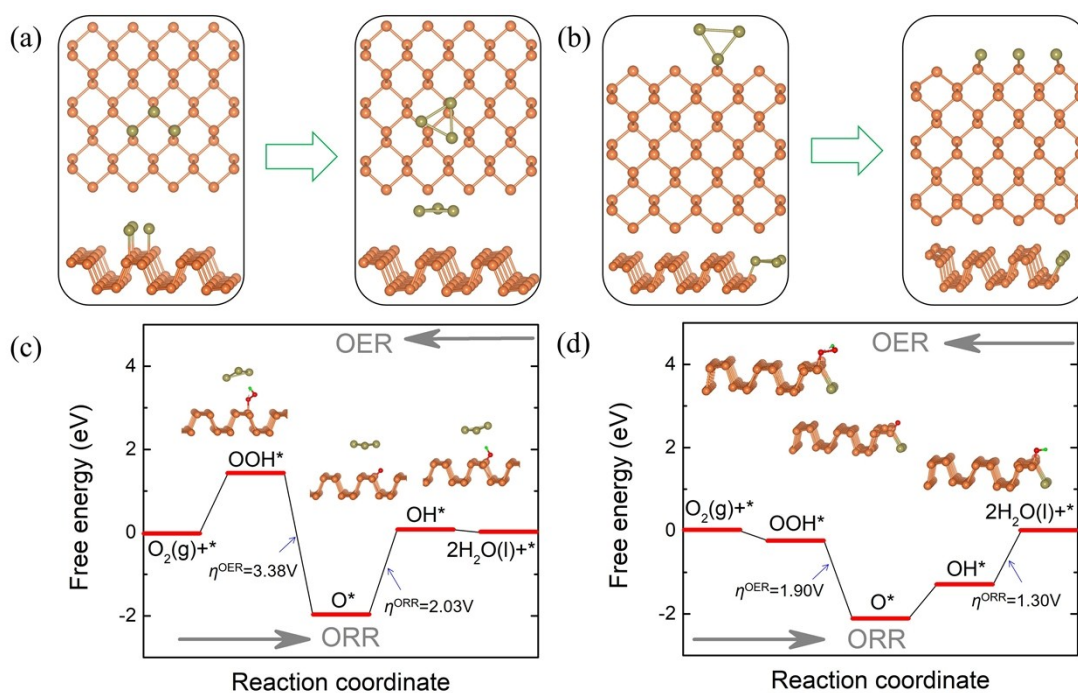


**Fig. S10** Atomic structures of Te clusters on (a) pristine phosphorene and (c) zigzag nanoribbons edges. The corresponding structures before structural relaxation are also shown. The free energy diagrams of (c) pristine phosphorene and (d) zigzag nanoribbons edges with adsorbed  $\text{Te}_p^x$  clusters at  $U = 0.402$  V. The adsorbed intermediates  $\text{O}^*$ ,  $\text{OH}^*$  and  $\text{OOH}^*$  are shown in insets.

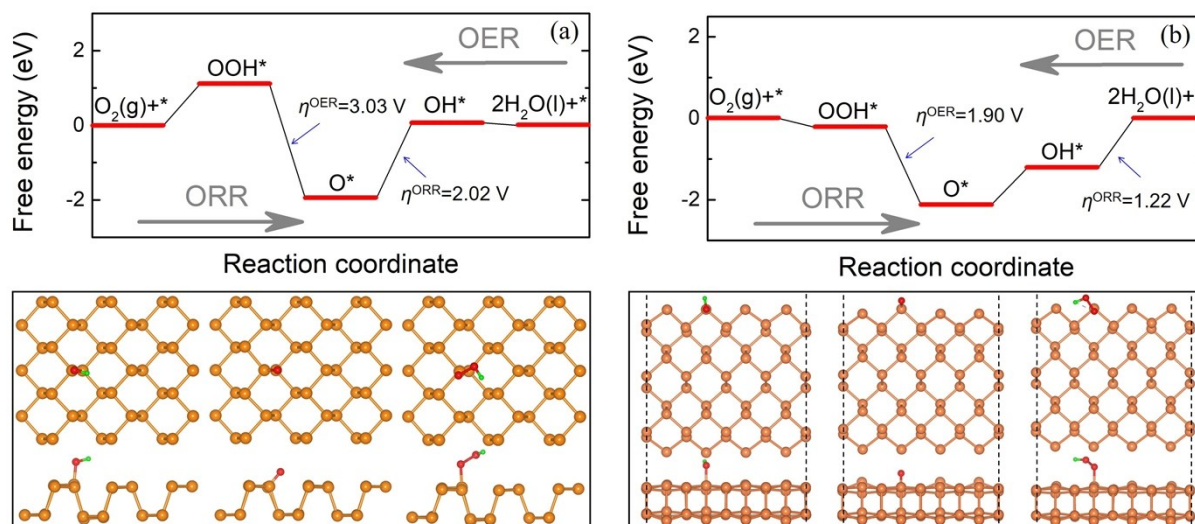


**Fig. S11** The free energy diagrams for ORR and OER pathways on (a) pristine phosphorene and (b) zigzag nanoribbon. The top and side view of corresponding structures with adsorbed intermediates  $\text{OH}^*$ ,  $\text{O}^*$ , and  $\text{OOH}^*$  are shown below each free energy diagram.

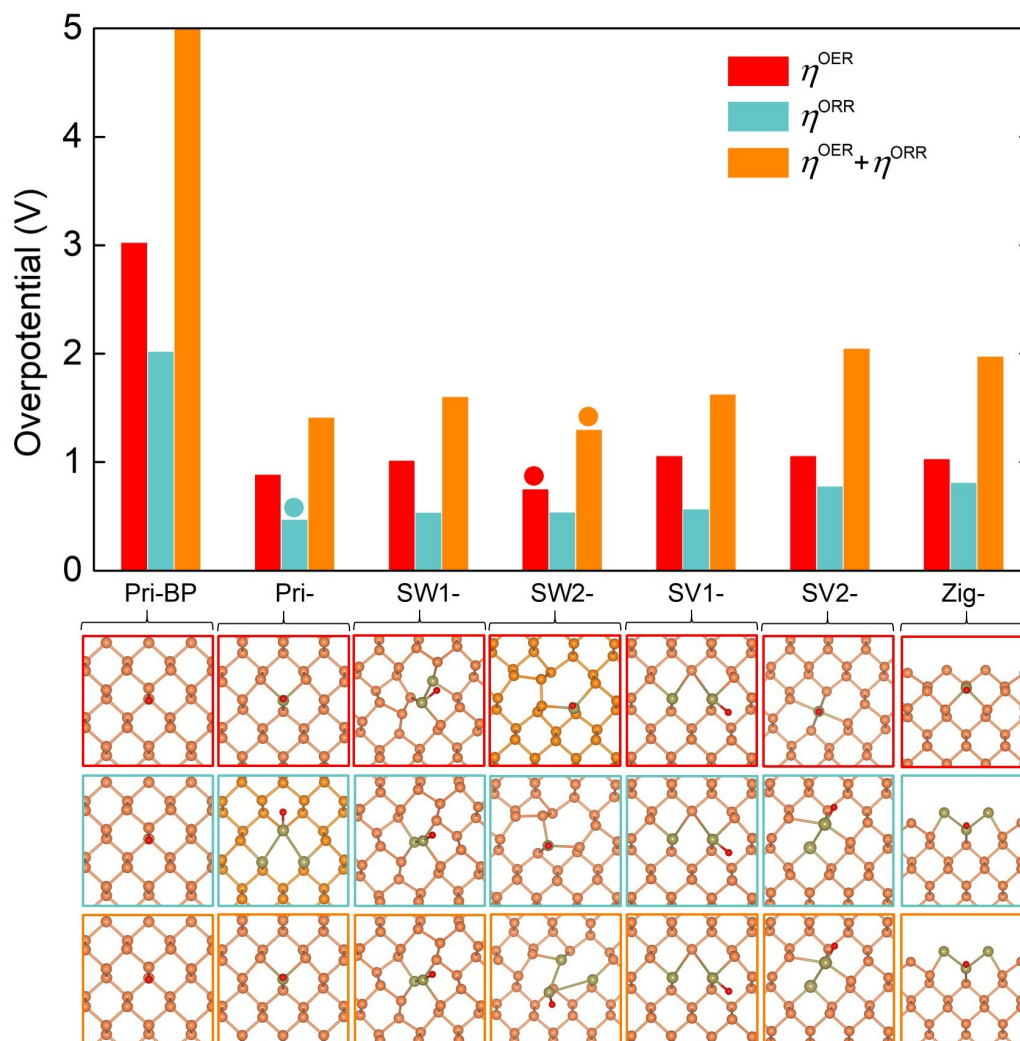


**Fig. S12** Optimal OER/ORR overpotentials and potential gaps ( $\eta^{\text{ORR}} + \eta^{\text{OER}}$ ) of pristine phosphene (Pri-BP), Pri-, SW-, SV- and Zig- $\text{Te}_p^x$  clusters. The corresponding atom structures with absorbed  $\text{O}^*$  are also shown below. Atom structures with optimal OER, ORR overpotentials and potential gaps are denoted by red, teal and brown borders, respectively.

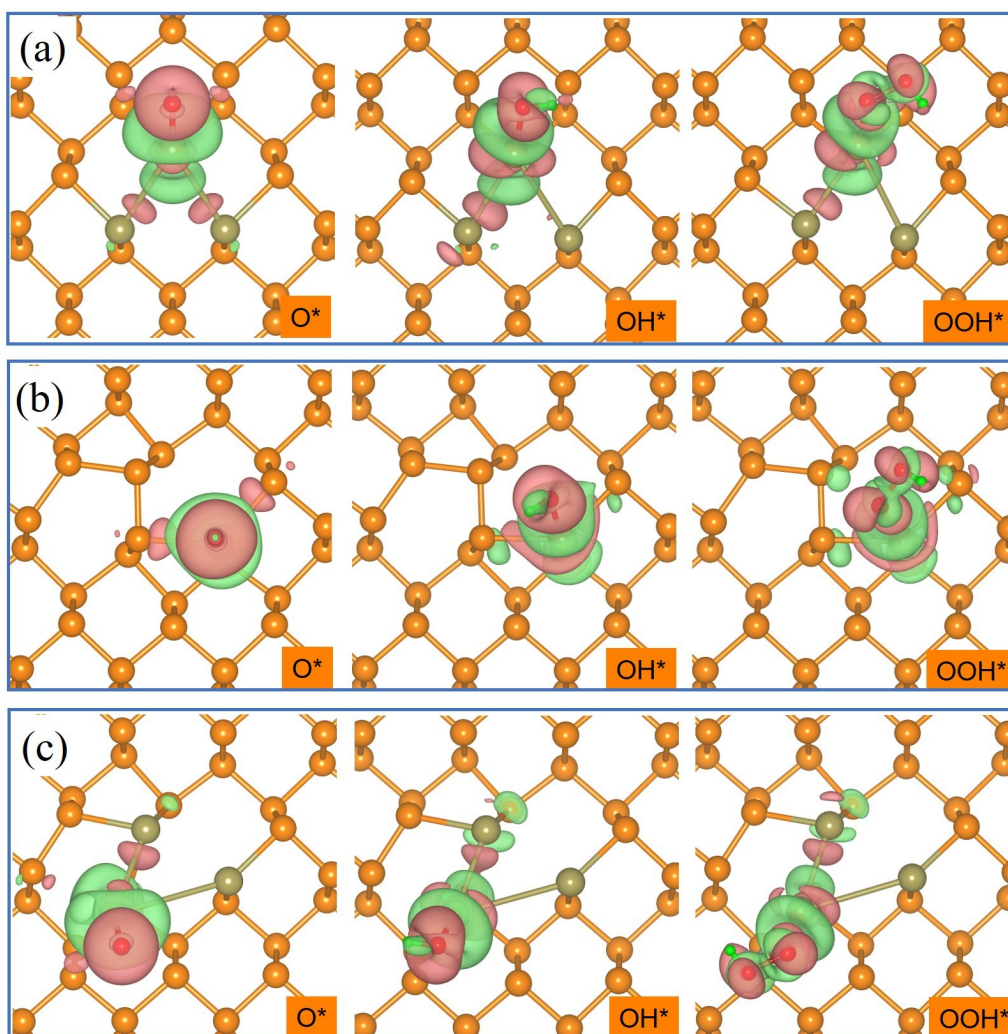


**Fig. S13** Charge density difference for O\*, OH\* and OOH\* on (a) Pri-Te<sub>p</sub><sup>3</sup>, (b) SW2-Te<sub>p</sub><sup>1</sup> and (c) SW2-Te<sub>p</sub><sup>3</sup> clusters. Light red (green) represent the charge gain (charge loss) and the iso-surfaces value is set as 0.002 e/Å<sup>3</sup>. For all structures, the strongest charge density transfers universally occur at intermediates (O\*, OH\* and OOH\*), active sites and neighbor atoms.

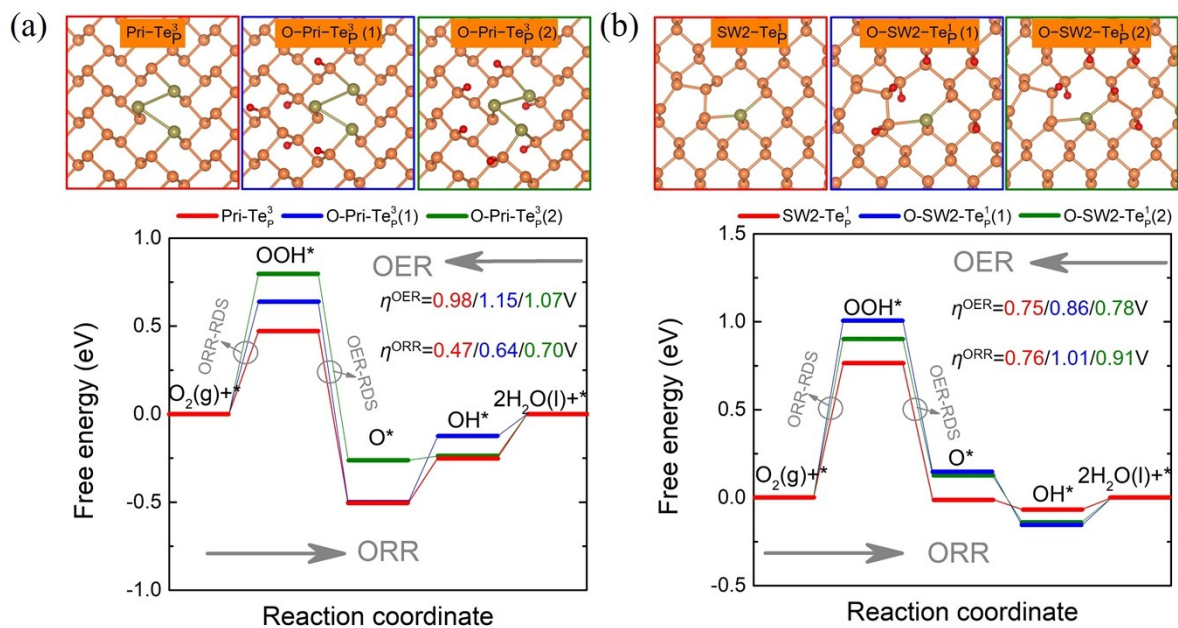


**Fig. S14** Atomic structures and free energy diagrams at  $U = 0.402$  V for (a) pure Pri-Te<sub>p</sub><sup>3</sup>, oxidic structures O-Pri-Te<sub>p</sub><sup>3</sup>(1) and O-Pri-Te<sub>p</sub><sup>3</sup>(2); and (b) pure SW2-Te<sub>p</sub><sup>1</sup>, oxidic structures O-SW2-Te<sub>p</sub><sup>1</sup>(1) and O-SW2-Te<sub>p</sub><sup>1</sup>(2). The calculated OER ( $\eta^{\text{OER}}$ ) and ORR ( $\eta^{\text{ORR}}$ ) overpotentials of pure and oxidic structures are denoted by red, blue and green numbers, respectively.

## References

1. I. C. Man, H.-Y. Su, F. Calle-Vallejo, H. A. Hansen, J. I. Martínez, N. G. Inoglu, J. Kitchin, T. F. Jaramillo, J. K. Nørskov and J. Rossmeisl, *ChemCatChem*, 2011, **3**, 1159-1165.
2. M. W. J. E. Chase, *J. Phys. Chem. Ref. Data, Monograph*, 1998, **9**.
3. M. Li, L. Zhang, Q. Xu, J. Niu and Z. Xia, *J. Catal.*, 2014, **314**, 66-72.